catalysts

MDPI

Article

Highly ordered Nanomaterial Functionalized Copper Schiff Base Framework: Synthesis, Characterization, and Hydrogen Peroxide Decomposition Performance

Fatemeh Rajabi [1,*], María Pinilla-de Dios [2] and Rafael Luque [2,*]

[1] Department of Science, Payame Noor University, P.O. Box 19395-4697, Tehran, Iran
[2] Departamento de Química Orgánica, Universidad de Córdoba, Edificio Marie Curie (C-3), Ctra Nnal IV-A, km 396, E14014 Córdoba, Spain; mpdedios@gmail.com
* Correspondence: f_rajabi@pnu.ac.ir (F.R.); q62alsor@uco.es (R.L.)

Received: 7 June 2017; Accepted: 12 July 2017; Published: 19 July 2017

Abstract: An immobilized copper Schiff base tridentate complex was prepared in three steps from SBA-15 supports. The immobilized copper nanocatalyst (heterogeneous catalyst) was characterized by Fourier transform infrared spectroscopy (FT-IR), cross polarization magic angle spinning (CP-MAS), 13-carbon nuclear magnetic resonance (^{13}C-NMR), atomic absorption spectroscopy (AAS), thermogravimetric analysis (TGA), and N_2-physisorption. Moreover, morphological and structural features of the immobilized nanocatalyst were analyzed using transmission electron microscopy (TEM) and X-ray powder diffraction spectrometry (PXRD). After characterizing the nanocatalyst, the catalytic activity was determined in hydrogen peroxide (H_2O_2) decomposition. The high decomposition yield of H_2O_2 was obtained for low-loaded copper content materials at pH 7 and at room temperature. Furthermore, the nanocatalyst exhibited high activity and stability under the investigated conditions, and could be recovered and reused for at least five consecutive times without any significant loss in activity. No copper leaching was detected during the reaction by AAS measurements.

Keywords: nanomaterials; immobilized copper Schiff base complex; hydrogen peroxide; decomposition; leaching

1. Introduction

The increase on environmental legislation as well as the aim to switch towards a more sustainable chemical industry (reducing industrial wastes) constitute big challenges for current chemical research [1]. Green Chemistry unifies concepts that include the design of novel and more environmentally friendly experimental methods in order to replace traditional, unsustainable chemistries.

Based on these premises, one innovative way that provides an elegant route to raise environmentally friendly processes is the use of immobilized catalysts as an alternative to homogeneous catalysts. These catalysts offer environmentally acceptable routes for the production of different chemicals. Reactions are normally cleaner with these types of catalysts, and can be carried out under mild reaction conditions. The insolubility of the support material offers many advantages over homogeneous catalysts, including an increasingly efficient recovery and reuse after reaction in any laboratory or industrial research. Immobilized catalysts also show more advantages over their homogeneous counterparts that include lower toxicity, easier handling, better reaction activity and selectivity, and a lower waste production [2–4].

Periodic mesoporous organosilicas (PMOs) are among the most promising supports to immobilize homogeneous catalysts. They exhibit highly-ordered porous and size-controlled structures, large specific surface areas, and they also present major accessibility and potential to be functionalized

with different functional chemical groups on their surface [5–11]. Due to their remarkable properties, these catalysts have found a significant variety of applications in catalysis, e.g., gas adsorption [12–16], energy conversion [17,18], organo-optoelectronics [19–22], energy storage [23,24], gas sensors [25,26], and drug delivery [27–29]. A common and very effective procedure for the synthesis of PMOs relates to the co-condensation of silica with precursors such as tetraalkoxysilane and trialkoxyorganosilane in the presence of a structure-directing agent (templating agent), which determines the structure features of the resulting materials. Consequently, organic groups can easily be incorporated in the pores of these materials via co-condensation [30–33].

Since the discovery of the first class of these mesoporous materials (MCM type [34]), all prepared using a surfactant template, this method has been extended to various types of mesoporous materials by different research groups. Extensive studies have been conducted on their synthesis, characterization, and applications [35–37]. In literature, different catalytic systems have been employed where hydrogen peroxide decomposition was carried out using 17.8 $g \cdot L^{-1}$ of H_2O_2 and 2.5 $g \cdot L^{-1}$ of bimetallic magnetic carbon xerogels with cobalt and iron microparticles at 50 °C and pH = 3 for 2 h. A maximum yield of 65% H_2O_2 decomposition was reported [38]. Bourlinos et al. studied the constant rate of hydrogen peroxide decomposition using Fe-doped carbon dots as a nanocatalyst, which was found to be 0.7×10^{-1} min^{-1} (with 10 mL 0.02 M of peroxide solution and 10 mg of Fe-doped carbon dots). An Fe(III)-functionalized carbon dot nanocatalyst was designed for this purpose (carbon dots (CDs), carbon-based materials) [39]. Tamami et al. studied a system based on a crosslinked polyacrylamide anchored Schiff base (1.9 mg copper content on the polymer support). The system could catalyze the decomposition of H_2O_2 (20 mL, 0.1 M) after 2 h with 100% conversion [40]. Additionally, Demetgül et al. reported an effective H_2O_2 decomposition over 4,6-diacetylresorcinol-chitosan-Cu(II) materials [41]. The reaction conditions involved 0.1 mmol catalyst Cu(II), 25 °C, 10 mL of a dissolution 3.5×10^{-2} M H_2O_2 and pH 6.86 for a reaction time of 60 min (90% conversion).

For these reasons, and taking into account our recent results related to the design of immobilized catalysts for organic transformations such as oxidation reactions and carbon-carbon bond formations [42–44], we report herein the synthesis of a novel Schiff base tridentate copper complex immobilized on mesoporous nanomaterials, Cu-L@SBA-15. The synthesized Cu-L@SBA-15 was characterized by techniques including transmission electron microscopy (TEM), Fourier transform infrared spectroscopy (FT-IR), cross polarization magic angle spinning (CP-MAS), 13-carbon nuclear magnetic resonance (^{13}C-NMR), X-ray powder diffraction spectrometry (PXRD), atomic absorption spectroscopy (AAS) and thermogravimetric analysis (TGA). Moreover, the catalytic performance of Cu-L@SBA-15 was investigated in hydrogen peroxide decomposition. Cu-L@SBA-15 revealed a strong catalytic activity towards the decomposition of H_2O_2 under the investigated conditions.

2. Results and Discussion

2.1. Morphology and Characterization of Immobilized Materials

Schiff bases synthesized from primary amine and carbonyl compounds have received significant attention in biological and coordination chemistry. Schiff base ligands are able to easily attach metal ions and to stabilize them in order to create highly stable coordination compounds [45–50]. Due to the biological essential activity of copper, its coordination chemistry has received significant attention. Particularly, a large number of Schiff base copper complexes have been developed to investigate their biological and catalytic potential [51–54]. The synthesis of a novel immobilized copper Schiff base complex was accomplished in three steps (Scheme 1). An SBA-15 support was prepared from pluronic P123 ($EO_{20}PO_{70}EO_{20}$, EO = ethylene oxide, PO = propylene oxide, Mn = 5800, Aldrich, Darmstadt, Germany) and tetraethoxysilane under acidic conditions. The resulting SBA-15 material was functionalized with *N*-(2-Aminoethyl)-3-(trimethoxysilyl) propylamine followed by condensation with pyridine-2 carbaldehyde to afford the corresponding immobilized Schiff base (L2@SBA-15). Finally, a complexation with copper acetate afforded the immobilized copper Schiff base nanocatalyst.

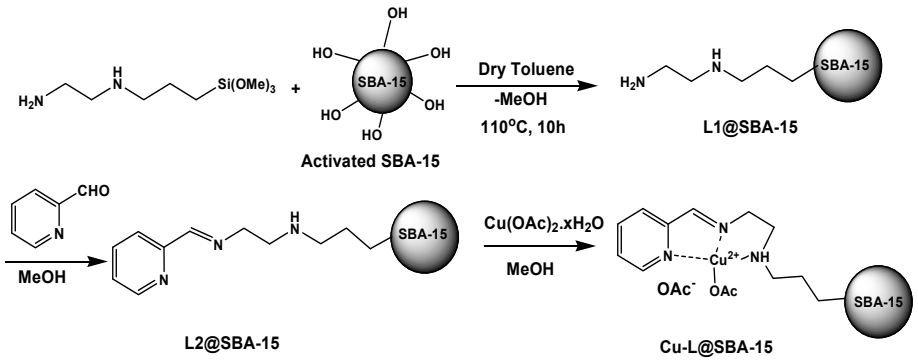

Scheme 1. Synthesis of the immobilized copper Schiff base nanocatalyst (Cu-L@SBA-15).

FT-IR was utilized to prove the incorporation of the Schiff base and copper species into the SBA-15 frameworks. FT-IR spectra of L2@SBA-15 and Cu-L@SBA-15 are shown in Figure 1. In the corresponding L2@SBA-15 spectra, Si-O-Si bands are located at ca. 800 and 1100 cm^{-1}, and are attributed to the symmetric and asymmetric Si-O-Si stretching of SBA-15, respectively. The silica network of SBA-15 was reported to exhibit a wide absorption band at 3430 cm^{-1}, attributed to the -OH stretching vibrations of silanol groups. The sharp stretching band at 2870 cm^{-1} is attributed to asymmetric and symmetric C-H stretching in the propyl chain. Stretching bands in the 1300–1600 cm^{-1} range are assigned to the vibrational modes of C=N, C=C, and C-H groups of the Schiff base moiety. N-H stretching could be observed at 3200 cm^{-1}. Similarly, the aforementioned bands were broadened and overlapped in the spectrum of Cu-L@SBA-15 due to the chelation of copper ions with the Schiff base. These results confirmed the successful functionalization of SBA-15 with a Schiff base and copper ions.

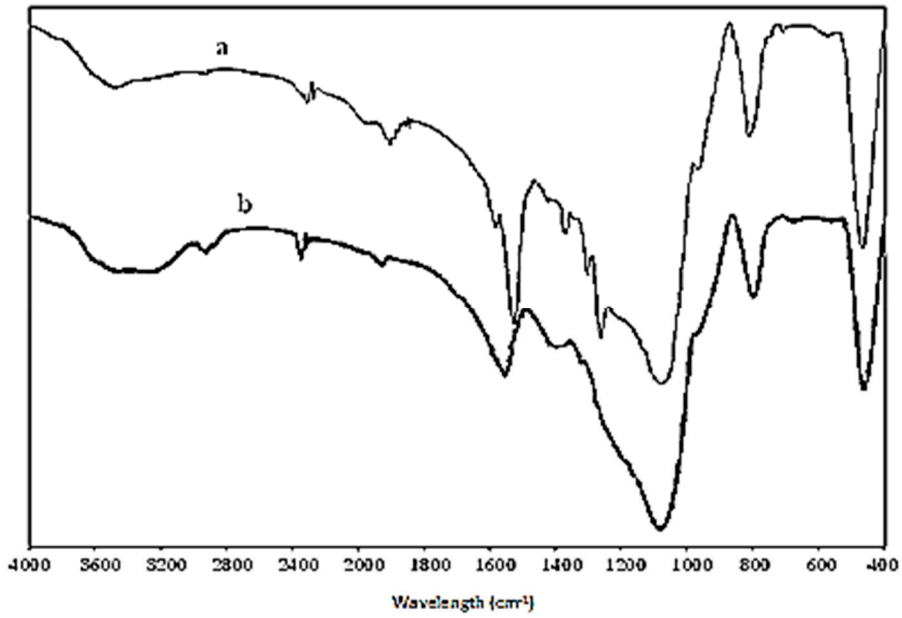

Figure 1. The FT-IR spectra of L2@SBA-15 (**a**) and Cu-L@SBA-15 (**b**).

More data supporting the formation of SBA-15 immobilized Schiff base copper complexes were obtained by solid-state ^{13}C-NMR spectrum of Cu-L@SBA-15 (Figure 2). ^{13}C-NMR spectra results of Cu-L@SBA-15 revealed that carbon resonances of *N*-(2-aminoethyl)-3-aminopropyl-chain could be observed at 10 (CH_2-Si), 20 (-CH_2-), and 40–55 (CH_2-NH-CH_2-CH_2-NH_2) ppm. In the aryl region,

a series of resonance signals found between 150 and 170 ppm could be attributed to pyridine rings. The peaks at 170–180 ppm could also be assigned to imine (C=N) groups of Schiff base moieties.

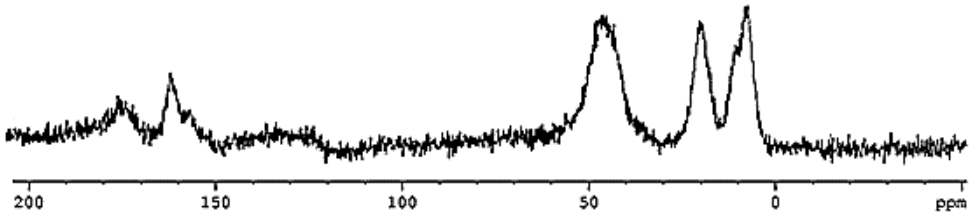

Figure 2. CP-MAS ^{13}C NMR spectrum of Cu-L@SBA-15.

The surface properties of the material were investigated by N_2-physisorption (Figure 3). Isotherms showed a hysteresis loop between (0.6–0.8) P/P_0 that indicates the mesoporosity of the sample with a bottle-neck geometry. The isotherm is of type IV with a type H1 hysteresis according to the International Union of Pure and Applied Chemistry (IUPAC) classification. The Brunauer–Emmett-Teller (BET) surface area and pore volume of Cu-L@SBA-15 were 346 $m^2 \cdot g^{-1}$ and 0.61 $cm^3 \cdot g^{-1}$, respectively, with a mean pore diameter of 8.55 nm.

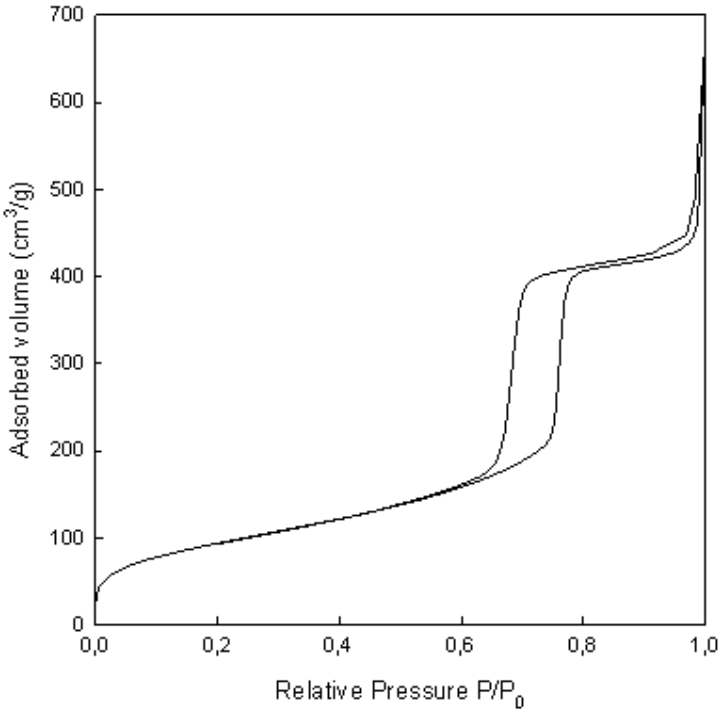

Figure 3. N_2 adsorption-desorption isotherms of Cu-L@SBA-15.

Further information about the thermal stability of Cu-L@SBA-15 could be extracted from TGA analysis data (Figure 4). Analyses were conducted from room temperature to 800 °C. Up to 200 °C, there is a relatively constant weight decrease (4.51%) due to the loss of water and organic solvent residues from the pore channels. The weight loss (57.73%) between 200 °C and 500 °C is generally attributed to the thermal dissociation of the functional organic moieties in the materials after grafting. The total 0.5 mol % weight loss of material amounts to 62.24%. This result indicates that Cu-L@SBA-15 has good thermal stability up to 400 °C. According to TGA analysis, the amount of copper Schiff base complex incorporated into the SBA-15 materials was 0.41 $mmol \cdot g^{-1}$.

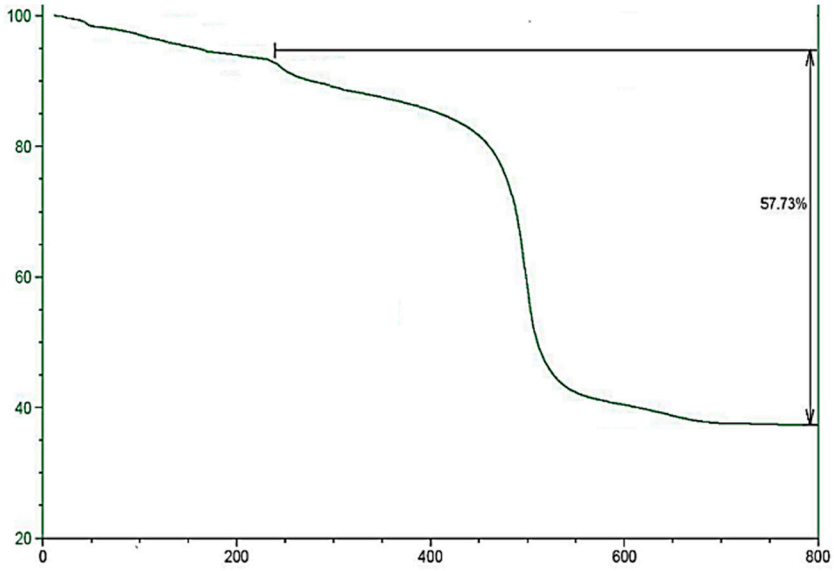

Figure 4. Thermogravimetric analysis of Cu-L@SBA-15.

Figure 5 shows the XRD pattern of Cu-L@SBA-15, which exhibits three distinctive peaks in the low-angle region. One intense signal corresponding to the d_{100} diffraction peak is accompanied by two weaker peaks (d_{110}, d_{200}), suggesting that the two-dimensional hexagonal (P6mm) pore structure is preserved after the introduction of the Schiff base copper complex.

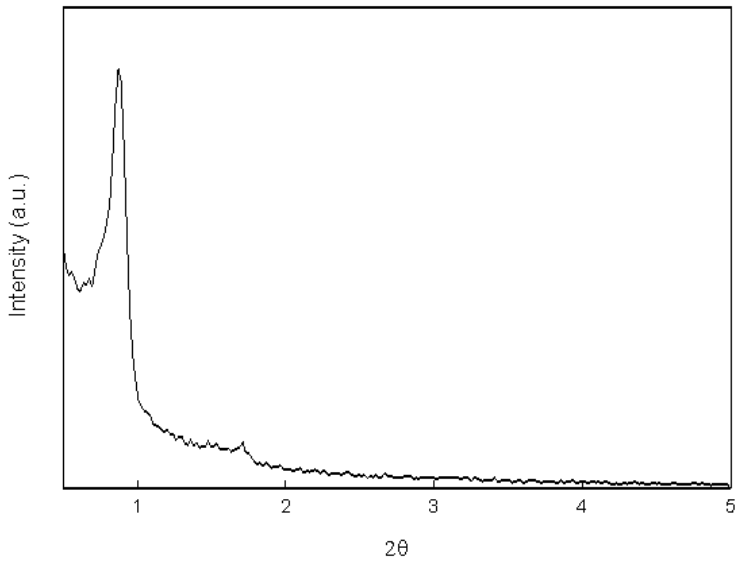

Figure 5. XRD pattern of Cu-L@SBA-15.

Further confirmation of the highly ordered mesostructure of the resulting material comes from TEM analysis. TEM images show a two-dimensional (2D) hexagonal arrangement of mesopores (Figure 6) which support the obtained results from PXRD analysis. Interestingly, TEM images also exhibit the presence of minor quantities of Cu nanoparticles (black dots, Figure 6) which were found to be present in very low concentrations, supporting the stable formation of the Schiff complex.

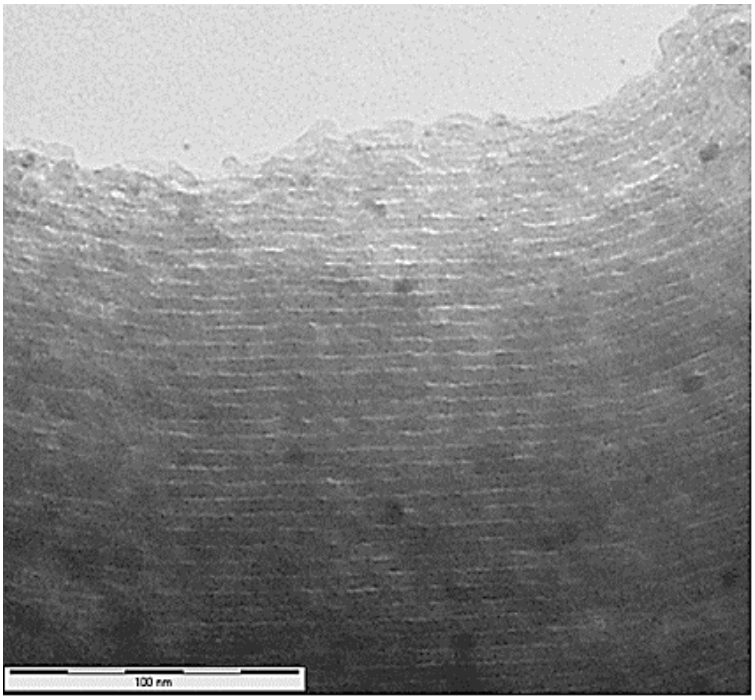

Figure 6. TEM image of Cu-L@SBA-15.

2.2. Catalytic Tests

The catalytic decomposition of hydrogen peroxide to oxygen and water has been extensively investigated by a variety of transition metal compounds and also by peroxidase enzymes found in many living media [55,56]. The decomposition rate of H_2O_2 is an important indicator to evaluate the catalytic activity of Cu-L@SBA-15. After the full characterization of Cu-L@SBA-15, the catalytic performance of the immobilized copper complex was examined by the decomposition of hydrogen peroxide under heterogeneous conditions. Different amounts of Cu-L@SBA-15 were used to investigate the effect of the variation in the amount of catalyst on the catalytic H_2O_2 decomposition performance. Plots of H_2O_2 decomposition at different amounts of Cu-L@SBA-15 nanocatalyst as a function of reaction time are given in Figure 7. Reactions were carried out in aqueous phosphate buffer, pH 7, at room temperature. Almost quantitative H_2O_2 decomposition was obtained using only 0.5 mol % of the supported copper nanocatalyst (Cu-L@SBA-15) in 50 min (Figure 7). Potassium permanganate ($KMnO_4$) was employed as an oxidizing agent to determine the amount of hydrogen peroxide in the solution. Blank runs (in the absence of the catalyst, and those performed only with the SBA-15 support and L1 and L2 systems) provided negligible decomposition activities under the investigated conditions. The hydrogen peroxide decomposition catalyzed by Cu-L@SBA-15 was kinetically monitored by an analytical titration of the residual H_2O_2 with KMnO4 solutions (0.05 M), standardized with sodium oxalate (primary standard). Hydrogen peroxide reduced the potassium permanganate to a colorless product. The chosen concentration of H_2O_2 was 0.05 M at pH 7. Furthermore, the studied range of the catalyst was from 0.001 mmol to 0.005 mmol Cu(II) at a constant concentration of H_2O_2, pH, and temperature. The decomposition was completed after 50 min (98% yield). The minimum amount of catalyst to ensure an optimum decomposition yield was found to be 0.005 mmol.

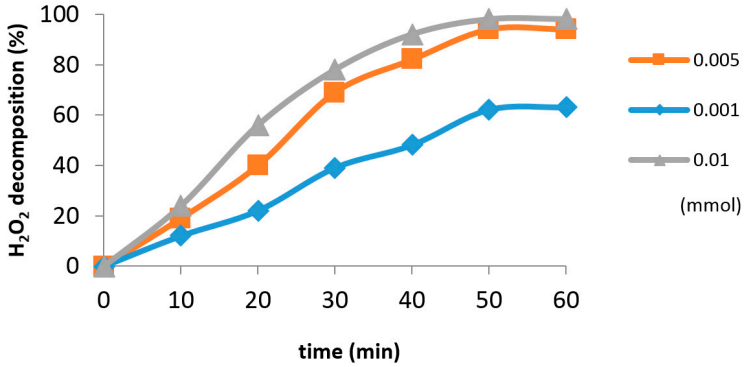

Figure 7. H_2O_2 decomposition using different amounts (mmol) of Cu-L@SBA-15 at room temperature.

2.3. Catalyst Reusability

The possibility of reuse of the immobilized catalyst is one of the most important features which determine the applicability of heterogeneous catalysts. To determine the stability and the reusability properties, the catalyst was separated from the reaction mixture after the first run, washed thoroughly with water and ethanol, and dried before its reuse in another reaction run. The Cu-based catalyst could be successfully reused five times without any appreciable loss in its catalytic activity. Filtrates were tested to determine any catalyst leaching by atomic absorption spectrometry. AAS results indicated that no leaching was observed during the first five consecutive runs. However, it was observed that after five runs, some copper was leached from the SBA-15 support (4 ppm, ca. 12%). Deactivation took place mostly due to the observed copper leaching from the support.

3. Experimental Section

3.1. Materials

All chemicals used in this study were purchased from Merck (Darmstadt, Germany) and were used as received without further purification, unless otherwise stated. Solid-state ^{13}C-NMR cross-polarization (CP) and magic angle spinning (MAS) spectra were recorded in a Bruker 300 MHz Ultrashield spectrometer (Rheinstetten, Germany). Nitrogen physisorption measurements were carried out at 77 K using an ASAP 2000 volumetric adsorption analyzer from Micromeritics (Micromeritics, Norcross, GA, USA). Samples were outgassed for 24 h at 100 °C under vacuum (10^{-4} mbar) and subsequently analyzed. Powder X-ray diffraction patterns were recorded on a Bruker-AXS diffractometer using Cu Kα radiation (λ = 1.5409 Å) (Rheinstetten, Germany). XPS measurements (Berlin, Germany) were performed in an ultra-high vacuum (UHV) multipurpose surface analysis system operating at pressures <10^{-10} mbar using a conventional X-ray source (XR-50, Specs, Mg-Kα, 1253.6 eV) in a "stop-and-go" mode to reduce potential damage due to sample irradiation. Powdered samples were deposited on a sample holder using double-sided adhesive tape, and subsequently released under vacuum (<10^{-6} mbar) overnight. TEM images were collected in a transmission electron microscope (Hitachi 200 kV electron beam energy, Tokyo, Japan) and TGA analysis was performed at a rate of 10 °C·min^{-1} in a temperature range of 25 to 800 °C under N_2 atmosphere using a NETZSCH STA 409 PC/PG Instrument (Selb, Germany). Metal content in the materials was determined using a Philips PU 9200 Atomic Absorption Spectrometer (AAS) (Almelo, The Netherlands). Samples were digested in HNO_3 and subsequently analyzed by AAS.

3.2. Preparation of L1@SBA-15

Synthesized SBA-15 was activated by refluxing with 6 M HCl for 12 h. It was filtered, washed with deionized water until neutral washings, and then dried in a vacuum oven at 60 °C for 10 h. Activated SBA-15 (2.0 g) was suspended in 50 mL of dry toluene. Then, 0.445 g (2 mmol)

of *N*-(2-Aminoethyl)-3-(trimethoxysilyl) propylamine was added dropwise to the suspension. The mixture was subsequently refluxed in toluene with a continuous removal of water using a Dean-Stark trap for 24 h. The slurry was filtered and the resulting mesoporous material (L1@SBA-15) was washed with an excess of hot toluene and ethanol in order to remove unreacted diamino silane precursor, and finally dried in a vacuum oven at 60 °C for 10 h to furnish L1@SBA-15 with a N loading ca. 0.55 mmol·g^{-1} (determined by TGA analysis).

3.3. Preparation of L2@SBA-15

For this preparation method, 1 mmol (0.107 g) of pyridine-2-carbaldehyde was added to the suspension of 1.0 g L1@SBA-15 in methanol (50 mL). The mixture was stirred under refluxed conditions for 24 h. The resulting yellow-colored solid was filtered, washed with an excess of methanol, and dried under vacuum conditions at 60 °C for 10 h to obtain L2@SBA-15 with a N loading of ca. 0.48 mmol·g^{-1} (determined by TGA analysis).

3.4. Preparation of Cu-L@SBA-15

To the stirred suspension of SG-SB1 (4.6 g) in methanol (50 mL), 0.145 g (0.8 mmol) of copper (II) acetate hydrate were added at 60 °C for 24 h, resulting in a green-colored solid material. After that, the solid phase was separated, washed with methanol, and dried under vacuum conditions for 24 h. The green solid was filtered and washed with 3 × 10 mL of methanol and subsequently dried in an oven at 60 °C overnight to furnish the corresponding nanocatalyst Cu-L@SBA-15 with a Cu loading of ca. 0.41 ± 0.01 mmol·g^{-1} (determined by TGA and AAS analysis).

3.5. General Procedure for Hydrogen Peroxide Decomposition

In a flask with a magnetic stirrer containing 50 mL of 0.05 M hydrogen peroxide solution in aqueous phosphate buffer pH7, 0.025 mmol of Cu-L@SBA-15 catalyst (62.5 mg) was added at room temperature. At constant pH, the decomposition of H_2O_2 was studied. The pH of the solutions was adjusted to 7 to obtain a neutral media, by using the buffer solution according to the reported literature. The extent of hydrogen peroxide decomposed at different intervals of time (intervals of 10 min from 0 to 60 min) was subsequently determined by taking 5 mL reaction mixture aliquots (filtered before analysis) and titrating them using 0.05 M $KMnO_4$ in the presence of 0.05 M H_2SO_4. The permanganate ion has a deep purple color, which disappeared after being consumed. The indication of the equivalence point occurred when the titrated solution had a light purple/pink color due to the slight excess of permanganate. To study the reusability of the catalyst, the immobilized copper catalyst was separated from the reaction mixture by simple filtration, then washed with water, and dried at vacuum conditions to be subsequently reused for the following run.

4. Conclusions

The design and synthesis of a highly-ordered mesoporous Schiff base tridentate copper complex (Cu-L@SBA-15) has been reported. The structure and physicochemical properties of Cu-L@SBA-15 were characterized by different analytical techniques such as FT-IR, XRD, TEM, CP-MAS, ^{13}C-NMR, AAS, TGA, and N_2-physisorption. The evaluated catalyst performance represents an environmentally benign and atom-economical process for hydrogen peroxide decomposition at room temperature, with further potential applications in several organic transformations. A complete decomposition of hydrogen peroxide takes place within 50 min using only 0.005 mmol of the catalyst. The studied catalyst could also be successfully recycled and reused without any significant loss of catalytic activity for five consecutive runs. Despite the high efficiency, stability, and reusability of the catalyst as well as low catalytic amounts required and a fast reaction rate under mild reaction conditions, the synthetic steps to design the reported catalytic system can be certainly improved from the green chemistry standpoint, with ongoing investigations in our group aimed to further advance the design of similar catalytic nanomaterials with better green credentials.

Acknowledgments: This work was partially supported by Payame Noor University.

Author Contributions: F.R. supervised and conducted all experimental work. All co-authors wrote, discussed, edited and commented on the manuscript. R.L. thoroughly revised and re-wrote the English of the manuscript in the revised version.

Conflicts of Interest: The authors declare no conflict of interest.

References

1. Clark, J.H. *Chemistry of Minimisation*; Blackie Academic: London, UK, 1995; pp. 17–64.
2. Clark, J.H. *Handbook of Green Chemistry and Technology*; Blackwell Science Ltd.: Oxford, UK, 2002; pp. 10–60.
3. Kirschning, A. *Immobilized Catalysts: Solid Phases, Immobilization and Applications*; Springer: Berlin, Germany, 2004; Volume 242, pp. 241–271.
4. Sherrington, D.C.; Kybett, A.P. *Supported Catalysts and Their Applications*; Royal Society of Chemistry: Cambridge, UK, 2001; pp. 48–54.
5. Zhao, D.; Feng, J.; Huo, Q.; Melosh, N.; Fredrickson, G.H.; Chmelka, B.F.; Stucky, G.D. Triblock copolymer syntheses of mesoporous silica with periodic 50 to 300 angstrom pores. *Science* **1998**, *279*, 548–552. [CrossRef] [PubMed]
6. DeVos, D.E.; Dams, M.; Sels, B.F.; Jacobs, P.A. Ordered mesoporous and microporous molecular sieves functionalized with transition metal complexes as catalysts for selective organic transformations. *Chem. Rev.* **2002**, *102*, 3615–3640. [CrossRef]
7. Taguchi, A.; Schìth, F. Ordered mesoporous materials in catalysis. *Microporous Mesoporous Mater.* **2005**, *77*, 1–45. [CrossRef]
8. Shea, K.J.; Loy, D.A.; Webster, O. Arylsilsesquioxane gels and related materials. New hybrids of organic and inorganic networks. *J. Am. Chem. Soc.* **1992**, *114*, 6700–6710. [CrossRef]
9. Loy, D.A.; Shea, K.J. Bridged polysilsesquioxanes. Highly porous hybrid organic-inorganic materials. *Chem. Rev.* **1995**, *95*, 1431–1442. [CrossRef]
10. Hoffmann, F.; Corne-lius, M.; Morell, J.; Fröba, M. Silica-based mesoporous organic-inorganic hybrid materials. *Angew. Chem. Int. Ed.* **2006**, *45*, 3216–3251. [CrossRef] [PubMed]
11. Sun, L.-B.; Liu, X.-Q.; Zhou, H.-C. Design and fabrication of mesoporous heterogeneous basic catalysts. *Chem. Soc. Rev.* **2015**, *44*, 5092–5147. [CrossRef] [PubMed]
12. Pater, J.P.G.; Jacobs, P.A.; Martens, J.A. Oligomerization of hex-1-ene over acidic aluminosilicate zeolites, MCM-41, and silica-alumina co-gel catalysts: A comparative study. *J. Catal.* **1999**, *184*, 262–267. [CrossRef]
13. Liang, Y.; Anwander, R. Nanostructured catalysts via metal amide-promoted smart grafting. *Dalton Trans.* **2013**, *42*, 12521–12545. [CrossRef] [PubMed]
14. Van Der Voort, P.; Esquivel, D.; De Canck, E.; Goethals, F.; Van Driessche, I.; Romero-Salguero, F.J. Periodic mesoporous organosilicas: from simple to complex bridges; a comprehensive overview of functions, morphologies and applications. *Chem. Soc. Rev.* **2013**, *42*, 3913–3955. [CrossRef] [PubMed]
15. Yang, Q.; Liu, J.; Zhang, L.; Li, C. Functionalized periodic mesoporous organosilicas for catalysis. *J. Mater. Chem.* **2009**, *19*, 1945–1955. [CrossRef]
16. Meng, X.; Nawaz, F.; Xiao, F.-S. Templating route for synthesizing mesoporous zeolites with improved catalytic properties. *Nano Today* **2009**, *4*, 292–301. [CrossRef]
17. Hata, H.; Saeki, S.; Kimura, T.; Sugahara, Y.; Kuroda, K. Adsorption of taxol into ordered mesoporous silicas with various pore diameters. *Chem. Mater.* **1999**, *11*, 1110–1119. [CrossRef]
18. Zhao, D.Y.; Yang, P.D.; Huo, Q.S.; Chmelka, B.F.; Stucky, G.D. Topological construction of mesoporous materials. *Curr. Opin. Solid State Mater. Sci.* **1998**, *3*, 111–121. [CrossRef]
19. Waki, M.; Maegawa, Y.; Hara, K.; Goto, Y.; Yamada, Y.; Mizoshita, N.; Tani, T.; Chun, W.-J.; Muratsugu, S.; Tada, M.; et al. A solid chelating ligand: periodic mesoporous organosilica containing 2, 2′-bipyridine within the pore walls. *J. Am. Chem. Soc.* **2014**, *136*, 4003–4011. [CrossRef] [PubMed]
20. Ciriminna, R.; Fidalgo, A.; Pandarus, V.; Béland, F.; Ilharco, L.M.; Pagliaro, M. The sol-gel route to advanced silica-based materials and recent applications. *Chem. Rev.* **2013**, *113*, 6592–6620. [CrossRef] [PubMed]
21. Linares, N.; Silvestre-Albero, A.M.; Serrano, E.; Silvestre-Albero, J.; García-Martínez, J. Mesoporous materials for clean energy technologies. *Chem. Soc. Rev.* **2014**, *43*, 7681–7717. [CrossRef] [PubMed]

22. Colmenares, J.C.; Luque, R. Heterogeneous photocatalytic nanomaterials: prospects and challenges in selective transformations of biomass-derived compounds. *Chem. Soc. Rev.* **2014**, *43*, 765–778. [CrossRef] [PubMed]
23. Morey, M.S.; Davidson, A.; Stucky, G.D. Silica-based, cubic mesostructures: Synthesis, characterization and relevance for catalysis. *J. Porous Mater.* **1998**, *5*, 195–204. [CrossRef]
24. Johnson-White, B.; Zeinali, M.; Shaffer, K.M.; Patterson, C.H.; Charles, P.T.; Markowitz, M.A. Detection of organics using porphyrin embedded nanoporous organosilicas. *Biosens. Bioelectron.* **2007**, *22*, 1154–1162. [CrossRef] [PubMed]
25. Lim, E.; Jo, C.; Lee, J. A mini review of designed mesoporous materials for energy-storage applications: from electric double-layer capacitors to hybrid supercapacitors. *Nanoscale* **2016**, *8*, 7827–7833. [CrossRef] [PubMed]
26. Wagner, T.; Haffer, S.; Weinberger, C.; Klaus, D.; Tiemann, M. Mesoporous materials as gas sensors. *Chem. Soc. Rev.* **2013**, *42*, 4036–4053. [CrossRef] [PubMed]
27. Moorthy, M.S.; Park, S.S.; Fuping, D.; Hong, S.H.; Selvaraj, M.; Ha, C.S. Step-up synthesis of amidoxime-functionalised periodic mesoporous organosilicas with an amphoteric ligand in the framework for drug delivery. *J. Mater. Chem.* **2012**, *22*, 9100–9108. [CrossRef]
28. Du, X.; Li, X.; Xiong, L.; Zhang, X.; Kleitz, F.; Qiao, S.Z. Mesoporous silica nanoparticles with organo-bridged silsesquioxane framework as innovative platforms for bioimaging and therapeutic agent delivery. *Biomaterials* **2016**, *91*, 90–127. [CrossRef] [PubMed]
29. Lee, C.-H.; Lin, T.-S.; Mou, C.-Y. Mesoporous materials for encapsulating enzymes. *Nano Today* **2009**, *4*, 165–179. [CrossRef]
30. Luque, R.; Balu, A.M.; Campelo, J.M.; Gracia, M.D.; Losada, E.; Pineda, A.; Romero, A.A.; Serrano-Ruiz, J.C. Catalytic applications of mesoporous silica-based materials. *Catalysis* **2012**, *24*, 253–280.
31. Karimi, B.; Mansouri, F.; Khorasani, M. Recent progress in design and application of functional ordered/periodic mesoporous silicas (OMSS) and organosilicas (PMOS) as catalyst support in carbon-carbon coupling reactions. *Curr. Org. Chem.* **2016**, *20*, 349–380. [CrossRef]
32. Polshettiwar, V.; Varma, R.S. Green chemistry by nano-catalysis. *Green Chem.* **2010**, *12*, 743–754. [CrossRef]
33. Prado, A.G.S.; Airoldi, C. Different neutral surfactant template extraction routes for synthetic hexagonal mesoporous silicas. *J. Mater. Chem.* **2002**, *12*, 3823–3826. [CrossRef]
34. Kresge, C.T.; Leonowicz, M.E.; Roth, W.J.; Vartuli, J.C.; Beck, J.S. Ordered mesoporous molecular sieves synthesized by a liquid-crystal template mechanism. *Nature* **1992**, *359*, 710–712. [CrossRef]
35. Melero, J.A.; van Grieken, R.; Morales, G. Advances in the synthesis and catalytic applications of organosulfonic-functionalized mesostructured materials. *Chem. Rev.* **2006**, *106*, 3790–3812. [CrossRef] [PubMed]
36. Huang, L.; Kruk, M. Versatile surfactant/swelling-agent template for synthesis of large-pore ordered mesoporous silicas and related hollow nanoparticles. *Chem. Mater.* **2015**, *27*, 679–689. [CrossRef]
37. Han, L.; Che, S. Anionic surfactant templated mesoporous silicas (AMSs). *Chem. Soc. Rev.* **2013**, *42*, 3740–3752. [CrossRef] [PubMed]
38. Ribeiro, R.S.; Silva, A.M.; Pinho, M.T.; Figueiredo, J.L.; Faria, J.L.; Gomes, H.T. Graphene-based materials for the catalytic wet peroxide oxidation of highly concentrated 4-nitrophenol solutions. *Catal. Today* **2015**, *249*, 204–212. [CrossRef]
39. Bourlinos, A.B.; Rathi, A.K.; Gawande, M.B.; Hola, K.; Goswami, A.; Kalytchuk, S.; Karakassides, M.A.; Kouloumpis, A.; Gournis, D.; Deligiannakis, Y.; et al. Fe(III)-functionalized carbon dots—Highly efficient photoluminescence redox catalyst for hydrogenations of olefins and decomposition of hydrogen peroxide. *Appl. Mater. Today* **2017**, *7*, 179–184. [CrossRef]
40. Tamami, B.; Ghasemi, S. Catalytic activity of Schiff-base transition metal complexes supported on crosslinked polyacrylamides for hydrogen peroxide decomposition. *J. Organomet. Chem.* **2015**, *794*, 311–317. [CrossRef]
41. Demetgül, C. Synthesis of the ketimine of chitosan and 4, 6-diacetylresorcinol, and study of the catalase-like activity of its copper chelate. *Carbohydr. Polym.* **2012**, *89*, 354–361. [CrossRef] [PubMed]
42. Rajabi, F.; Karimi, N.; Saidi, M.R.; Primo, A.; Varma, R.S.; Luque, R. Unprecedented selective oxidation of styrene derivatives using a supported iron oxide nanocatalyst in aqueous medium. *Adv. Synth. Catal.* **2012**, *354*, 1707–1711. [CrossRef]

43. Rajabi, F.; Nourian, S.; Ghiassian, S.; Balu, A.M.; Saidi, M.R.; Serrano-Ruiz, J.C.; Luque, R. Heterogeneously catalysed Strecker-type reactions using supported Co (II) catalysts: Microwave vs. conventional heating. *Green Chem.* **2011**, *13*, 3282–3289. [CrossRef]
44. Rajabi, F.; Schaffner, D.; Follmann, S.; Wilhelm, C.; Ernst, S.; Thiel, W.R. Electrostatic grafting of a palladium n-heterocyclic carbene catalyst on a periodic mesoporous organosilica and its application in the Suzuki-miyaura reaction. *ChemCatChem* **2015**, *7*, 3513–3518. [CrossRef]
45. Yang, M.; Zhang, X.; Grosjean, A.; Soroka, I.; Jonsson, M. kinetics and mechanism of the reaction between H_2O_2 and tungsten powder in water. *J. Phys. Chem. C* **2015**, *119*, 22560–22569. [CrossRef]
46. Jia, Y.; Li, J. Molecular assembly of Schiff base interactions: Construction and application. *Chem. Rev.* **2015**, *115*, 1597–1621. [CrossRef] [PubMed]
47. Casellato, U.; Vigato, P.A. Transition metal complexes with binucleating ligands. *Coord. Chem. Rev.* **1977**, *23*, 31–50. [CrossRef]
48. Gupta, K.C.; Sutar, A.K.; Lin, C.C. Polymer-supported Schiff base complexes in oxidation reactions. *Coord. Chem. Rev.* **2009**, *253*, 1926–1946. [CrossRef]
49. Cozzi, P.G. Metal-Salen Schiff base complexes in catalysis: Practical aspects. *Chem. Soc. Rev.* **2004**, *33*, 410–421. [CrossRef] [PubMed]
50. Gupta, K.C.; Sutar, A.K. Catalytic activities of Schiff base transition metal complexes. *Coord. Chem. Rev.* **2008**, *252*, 1420–1450. [CrossRef]
51. Liu, X.; Novoa, N.; Manzur, C.; Carrillo, D.; Hamon, J.-R. New organometallic Schiff-base copper complexes as efficient "click" reaction precatalysts. *New J. Chem.* **2016**, *40*, 3308–3313. [CrossRef]
52. Yu, H.; Yang, Y.; Li, Q.; Ma, T.; Xu, J.; Zhu, T.; Xie, J.; Zhu, W.; Cao, Z.; Dong, K.; et al. Ternary dinuclear copper (II) complexes of a reduced schiff Base ligand with diimine coligands: DNA binding, cytotoxic cell apoptosis, and apoptotic mechanism. *Chem. Biol. Drug Des.* **2016**, *87*, 398–408. [CrossRef] [PubMed]
53. Golcu, A.; Tumer, M.; Demirelli, H.; Wheatley, R.A. Cd (II) and Cu (II) complexes of polydentate Schiff base ligands: synthesis, characterization, properties and biological activity. *Inorg. Chimica Acta* **2005**, *358*, 1785–1797. [CrossRef]
54. Chaviara, A.T.; Cox, P.J.; Repana, K.H.; Pantazaki, A.A.; Papazisis, K.T.; Kortsaris, A.H.; Kyriakidis, D.A.; Nikolov, G.S.; Bolos, C.A. The unexpected formation of biologically active Cu(II) Schiff mono-base complexes with 2-thiophene-carboxaldehyde and dipropylenetriamine: Crystal and molecular structure of $CudptaSCl_2$. *J. Inorg. Biochem.* **2005**, *99*, 467–476. [CrossRef] [PubMed]
55. Spear, E.B. Catalytic decomposition of hydrogen peroxide under high pressures of oxygen. *J. Am. Chem. Soc.* **1908**, *30*, 195–209. [CrossRef]
56. McKee, D.W. Catalytic decomposition of hydrogen peroxide by metals and alloys of the platinum group. *J. Catal.* **1969**, *14*, 355–364. [CrossRef]